Polytechnic Journal. 2022. 12(1): 155-162
ISSN: 2313-5727
http://journals.epu.edu.iq/index.php/polytechnic

RESEARCH ARTICLE

Synthesis and Characterization of Au/ Sb_2O_3 Ultrathin nanosheet/Au as a High-Performance UV-Photodetector

Nageb T. Rassam [1]

[1] *Department of Technical Information System Engineering, Erbil Technical Engineering College, Erbil Polytechnic University, Erbil, Kurdistan Region, Iraq*

***Corresponding author:**
Nageb T. Rassam, Department of Technical Information System Engineering, Erbil Technical Engineering College, Erbil Polytechnic University, Erbil, Kurdistan Region - Iraq.

E-mail:
nageb.rassam@epu.edu.iq

Received: 15 May 2022
Accepted: 2 June 2022
Published: **14** August 2022

DOI
10.25156/ptj.v12n1y2022.pp155-162

ABSTRACT

Ultrathin antimony trioxide (Sb_2O_3) was synthesized on ITO substrate by a solvothermal method using ethanol as a solvent. The structure, morphological variations, and optical properties of the as-prepared sample were characterized. The results indicated that the homogeneously grown sheet of cubic phase of ultrathin Sb_2O_3 has an elliptical cross-section with a thickness of 20 nm and diameter of 400-500 nm. Further, an ultraviolet (UV) performance photodetector based on the (Au/Sb_2O_3/Au) was fabricated and examined. The measured Current-Voltage (IV) curves in the dark and under illumination (UV-395 nm) of different intensities indicate the presence of the Schottky barrier at the interfaces between Sb_2O_3 and Au-electrodes. Photocurrent values of 2.32, 16.5, and 25.58 μA were obtained for intensities of 4, 8 and 12 mW/cm^2, respectively at bias voltage of +3V, as compared to a dark current of 0.78μA. Sensitivity and responsivity values of 40.04 and 6.294W/A were recorded. The current-time (I-T) graph was utilized to derive the response and recovery times of the sensor under chopped UV-laser at different power intensities. The sensor exhibited fast response and recovery times of 113.6 ms and 67.2 ms, respectively, making this a high-performance sensor. This study demonstrates that ultrathin Sb_2O_3 nanosheet can be very useful to develop simple and high-performance UV sensors in different commercial fields and industries in the future.

Keywords: Sb_2O_3; Ultrathin nanosheets; Au/Sb_2O_3/Au; MSM UV-photodetector

1. INTRODUCTION

Photodetectors are essentially semiconductor devices that are based on the conversion of incident optical signals into electrical signals (photocurrent). The photodetection of the optical signals across a fraction of the electromagnetic (EM) spectrum is typically defined according to the material properties. The significance of the ultraviolet (UV) photodetector is rooted in its application in a variety of areas that include bio-analysis, optical communication, space and military purpose. According to their different working mechanisms or device structures, photodetectors can be divided into several groups, such as photoconductive, Schottky barrier, p-n junction, p-i-n junction, phototransistor, and metal-semiconductor-metal (MSM) photodetectors. With regard the photodetector device configuration, the simple and economical production of MSM photodetectors that consist of two interdigitated Schottky electrode contacts on their planar semiconductor surfaces has garnered considerable interest because of their low dark currents, low noise, rapid response, and absence of dopants. This explains the recent Proliferation of wide bandgap metal oxides and their devices. Metal oxides such as ZnO, TiO_2 , SnO_2 , NiO, Ga_2O_3 , and Sb_2O_3 have been investigated for application in high-performance UV photodetection. Antimony trioxide (Sb_2O_3), a vital wide band gap semiconductor, can be potentially applied as an optical material, functional filler, catalyst, and highly efficient fire-resistant synergist in the manufacture of adhesives, plastics and paints. In addition to its band gap (3.35 eV), the facile synthesis of Sb_2O_3 material with diverse morphologies is an additional benefit, like high-efficiency solar energy conversion and gas-sensing performance. The properties of Sb_2O_3 depend on its chemical compositions, shapes and sizes. Recently, there has been more publications on the morphology-controlled production of complex Sb_2O_3 nanomaterials with distinct morphologies using different approaches that include hydrothermal or solvothermal methods. The nanosheet morphology has shown to be an ideal 2D material that is attributed to its relatively large surface area which offers sufficient active sites that can enhance the mobility of surface electrons. it exhibits exceptional applications in the areas of energy and the environment.

Few types of research have been done using Sb_2O_3 as a base of MSM UV-photodetector, such as Au/Sb_2O_3 nanobelt networks and Sb_2O_3/Ag/Sb_2O_3 multilayer. Herein, ultrathin Sb_2O_3 nanosheets were successfully synthesized using a simple solvothermal synthesis technique. In this work the structure, morphology and optical properties were provided. Afterwards an (MSM) UV- photodetector synthesized based on Sb_2O_3 by deposition of Au electrode on its surface. The photoconductive applications of (Au/Sb_2O_3/Au) are featured by: fast response and decay time, high sensitivity, and excellent repeatability.

2. Materials and Methods

2.1. Sb_2O_3Nanosheet synthesis

Antimony trichloride ($SbCl_3$, Sigma-Aldrich, Assay 99.95%) was utilized as a source of the antimony with a molarity of 0.01M, where 2.88 g of $SbCl_3$ was dissolved in 100 ml ethanol. Few drops of NHO_3 were added to the solvent to adjust the pH value to (8-9) of the solution. The mixture was stirred under ambient conditions by means of a magnetic stirrer for 20 min. Then, 75 ml of the mix solution was transferred into a 100 ml Teflon-lined stainless-steel autoclave that contains the substrate i.e. indium tin oxide (ITO) (Zhuhai kaivoelectronic company Co., Ltd, surface resistance <15Ω/□ and transmittance > 85%). The substrate was washed with double distilled water and was immersed in a solution containing 10% HCl and 90% water for 1 min. After that, the substrate was cleaned with double distilled water. The ITO was placed next to the Teflon-lined wall and then immersed in the solution. The airtight autoclave was placed inside an electric oven at 180 °C for 6 h and gradually cooled to room temperature, the film was washed with deionized water and pure alcohol several times and dried after that at 60 °C for 2 h.

2.2. Characterization techniques

The crystal structure and morphological variations of the as prepared Sb_2O_3 deposited on ITO substrate were characterized. The crystallinity and phase purity of the samples were investigated using 2θ range of 10-80° using X-ray diffractometer (XRD) (Burker D8 advance) with Cu-kα radiation (λ = 1.54178 Å). Morphological variations and elemental compositions of the samples were studied using Field-emission scanning electron microscopy (FESEM). Ultra violet-visible-near infrared spectrophotometer (UV-VIS-NIR) (Cary 5000) was utilized to determine the optical properties of the synthesized Sb_2O_3 nanosheet in the reflection spectra range of 200-1000 nm. Electrical contacts are made using the thermal evaporation coating system type (JEE-4B/4C). The metal Au was deposited on the front Sb_2O_3 films through the mask consisting of an interdigitated electrode with five fingers. The Au metal was deposited on the front side of Sb_2O_3 that grows on ITO, where the current flows laterally through the contacts. The schematic diagram of Au/Sb2O3 nanosheet/Au configuration and the experimental setup is shown in Fig.1.

In order to characterize the prepared UV-photodetector, an experiment was setup, as shown schematically in Fig.1, to obtain dark and illuminated I-V curves for different UV intensities. The set-up consists of the light illumination source UV- LED laser with wavelength 395 nm and different

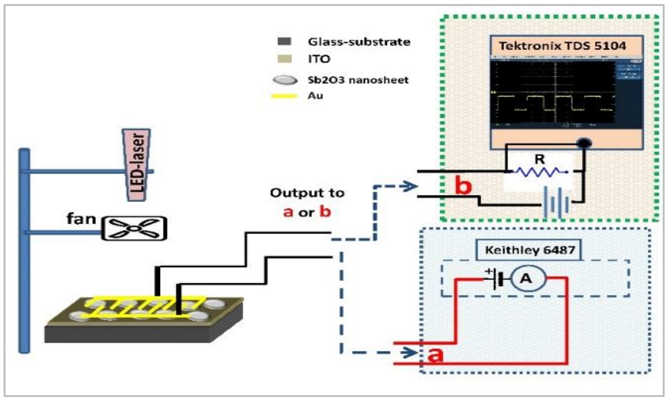

Fig. 1 Electric circuit for measurement dark and light I-V of

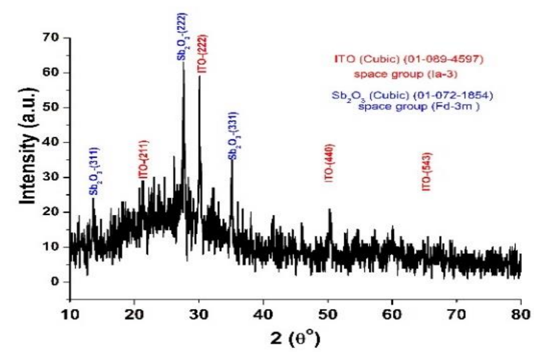

Fig. 2 XRD pattern of Sb2O3 nanosheet deposited on ITO substrate by solvothermal method.

intensities (4, 8, 12 mW/cm^2) mounted at 20 cm above the sample. The laser beam was chopped by a fan to derive an on/off light reference. Based on the measured I-V curves, the sensitivity, responsivity, response (rise), and recovery (fall) time of the sensor were derived by connecting to one of the two sub-parts (a) or (b),

Connection to the sub-part (a);

This section covers the measurement of current voltage (I-V), where the device is directly connected to a picometer voltage source (model: Keithley 6487). The procedure begins with measuring the I-V curves at dark and under light (with illumination) at room temperature when the fan is disconnected.

Connection to the sub-part (b);

This part measures the response (rise) and the recovery (fall) time of the photodetector. The voltage of the sampling resistor, which is reflective of photocurrent change in the detector, was constantly recorded using a computerized oscillograph (Tektronix TDS 5104). The obtained signals were subsequently converted to achieve these sensitivity parameters (rise and fall times) of the sensor. In this part, both the light source and fan were turned "on" and the differences in output current signals versus time (I-t) at bias voltage of +5 V were measured at room temperature under illumination.

3. Results and discussion

3.1 Morphology and structures analysis

Fig. 2 illustrates the XRD pattern of as prepared Sb_2O_3 growth over ITO substrate. The diffraction peak at 2θ of (27.66 °) corresponds to the (222) plane. The other two peaks at 2θ of (13.69 °, 35.16 °) barely rise out of the noise background, but also match the standard cubic Sb_2O_3 pattern which corresponds to the (311) and (331) planes, respectively. These diffraction peaks are characteristic of Sb_2O_3, as they match well with those of the standard cubic Sb_2O_3 pattern (ICSD-: 01-072-1854). The high intensity and distinct XRD peak of (222) plane indicate well crystallization of the as-synthesized product. In addition, four other weak peaks at 21.18 °, 30.12 °, 50.43 °, and, 65.10 ° which are assigned to the (211), (222), (440), and (543) planes, respectively, match with the cubic ITO substrate (ICSD-: 01-089-4597). The characteristic peaks of metallic Sb or any other phases were indiscernible.

Fig. 3 shows different magnifications of the top view FESEM images of Sb_2O_3 nanosheets grown on the ITO substrate. The FESEM images were analyzed.

It was observed that an assembly of needle like structure or

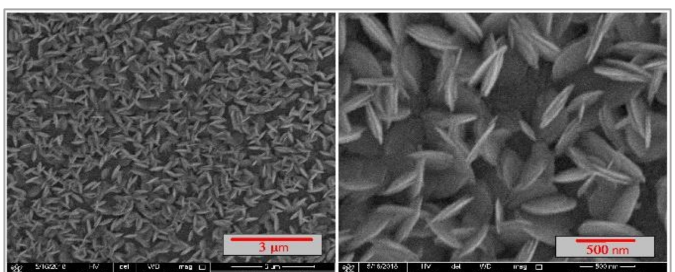

Fig. 3 Top view FESEM images with different magnifications for Sb_2O_3 nanosheet growth on ITO substrate.

platelet like structures grew homogenously on ITO surface. The dimensions of needle or platelet like structures have been measured by using scanning probe image processing (SPIP) software. The average thickness of (20) nm and elliptical cross section diameter of (400-500) nm was recorded. The array of novel morphologies of Sb_2O_3 crystals comprises nanosheets, nanorods, nanowires, nanobelts, belt-like, flower-like, bundle-like and cubic-like, hollows spindle-like/cobble, stone-like, and microspheres Sb_2O_3.

The EDX spectrum of the Sb_2O_3 growth on ITO is depicted in Fig. 4. The EDX confirms the Sb and O elements. Atomic percentages of Sb and O are 14.6 and 62.41. In addition, Indium (In), Silicon (Si) and the high value of oxygen (O) were resulted from substrate compound of (ITO and Glass), in addition to that presents in Sb_2O_3 nanosheet. The results of structure, morphology, EDX and XRD indicate that Sb_2O_3 could be growth very thin in the range of nanoscale on the ITO substrate.

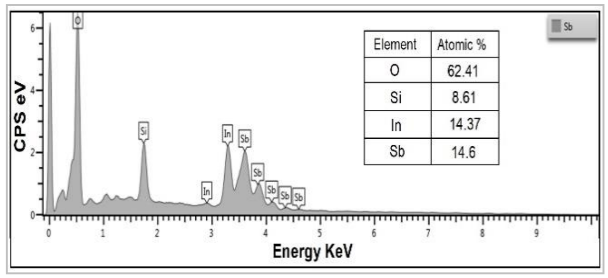

Fig. 4. EDX spectrum of the Sb_2O_3 nanosheet/ITO. The inset table illustrated the atomic % of elements.

3.2 Optical analysis

UV-VIS-NIR was used to obtain the reflection (diffusion) spectra of Sb_2O_3 nanosheet in the range (200-1000) nm, as shown in Fig. 5.

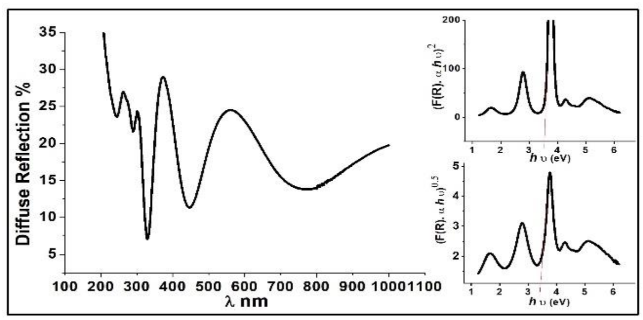

The Kubelka-Munk relation was utilized to match the reflectance data with the absorption coefficient. This relation relates the reflectance data to the absorption coefficient based on the following equation:

$$F(R) = \frac{\alpha}{s} = \frac{(1-R)^2}{2R} \quad \text{........} \quad (1)$$

where F(R), R, α and s denote the Kubelka-Munk function, reflectance, absorption coefficient and scattering factor, respectively.

The modified Kubelka–Munk function can be derived from the multiplication of F(R) and hv using the corresponding coefficient (n) which can be related to an electronic transition according to:

$$F(R).\, h\nu = k(h\nu - E_g)^n \quad \text{.........}(2)$$

where k and Eg represent energy-independent constant and optical energy gap, respectively. The exponent n is dependent on the type of transition. The n values of 1/2 and 2 are for direct and indirect allowed transitions, respectively.

The bandgap energy was derived from the plot of $(F(R).\ h\nu)^n$ versus hν by extrapolating the linear region of the gradient to $F(R) \rightarrow 0$

As inferred from the UV-Vis-NIR transmission spectrum, the bulk Sb_2O_3 phase has an indirect energy bandgap of 3.30 eV. Fig. 5 shows the diffuse reflectance I spectra of the Sb_2O_3 nanosheet grown on ITO. The spectra display relatively low reflection (high absorption) at 330 nm, and a high reflection (weak absorption) around 420 nm indicates a high light scattering. The inset in Fig. 5 shows the plots for the derivation of E_g according to relation (2). The direct E_g for the ultrathin Sb_2O_3 nanosheets is 3.6 eV. Due to its average thickness of 20 nm and elliptical cross-section diameter of 400-500 nm. This Eg differs significantly from that of the bulk phase. Similar results were reported by Z. Deng et al., in their study of the photoluminescence of rectangular Sb_2O_3 nanowires. The E_g of the Sb_2O_3 ultra-thin nanosheet prepared in this study is close to that of ZnO, which supports its potential application in the manufacture of optical and electronic nanodevices, like photodiodes, light-emitting diodes, solar cells, catalysts, flame retardants, chemical sensors, etc.

3.3 Photodetection analysis

As the illumination photon energy exceeds the energy band gap (3.6 eV) of Sb_2O_3 nanosheet, electron-hole pairs are produced. One type of carrier is usually trapped at or near the surface region, while the other type is dispelled by the applied bias and accumulated at the electrode, which explains the enhanced conductivity under illumination. In addition, the usual division of carrier types has a tendency to boost their life span, resulting in enhanced photodetection performance of the Sb_2O_3.

Photodetection properties were investigated by measuring (I-V) curves using the system shown in Fig.1**.** Fig. 6 shows I-V curves of (Au/Sb_2O_3 nanosheet/Au) device measured under a UV-LED (395 nm) and in the dark. These curves were obtained under different UV

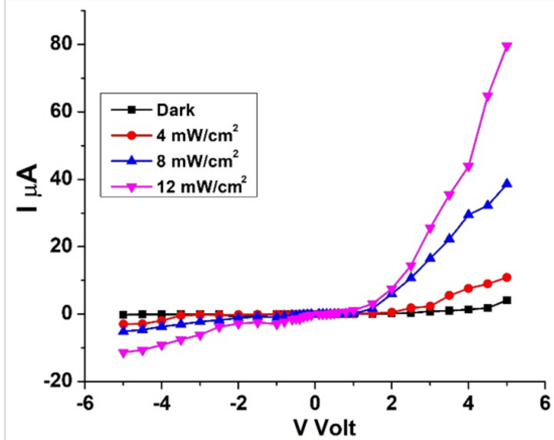

Fig. 6: forward and reveres bias Dark and light I-V characteristics of Au/ nanosheet Sb_2O_3/Au.

intensities (4, 8, and 12 $W.m^{-2}$) at the bias voltage range of (-5V to +5V). The dark current is 0.78 µA, whereas the photocurrent values are 2.32, 16.5, and 25.58 µA for UV intensities of 4, 8, and 12 mW/cm^2, respectively, at a bias voltage of +3V. The photo-excited current is (~3 - 30) times higher than the dark current. Moreover, the nonlinear I-V curve indicates that Schottky barriers exist at the interfaces between the photodetector surfaces (Sb_2O_3 nanosheet) and the electrodes since the current passes laterally through the device. No transition from the Schottky barrier to ohmic contact characteristics was observed,

The sensitivity (S) and responsivity ($\Re$) of the photodetector were obtained from I-V curves, where sensitivity is measured using the following equation:

$S = I_{ph}/I_{dark}$, ……….. (3)

where, $I_{ph} = I_{light} - I_{dark}$.

Fig. 7 (a) shows the forward and reverse bias photosensitivity for Au/Sb_2O_3/Au device with bias voltages in the range of -5 to +5 V at different intensities of incident UV light (4, 8, 12) mW/cm^2. As observed in Fig. 7 (a), the photosensitivity of the MSM device increases with light intensity for both forward and reverse biased voltages. The maximum sensitivity was found to be 40.04 at bias voltage of +4 V. The sensitivity decreases beyond this value for forward bias voltage. This is attributable to increase in dark current with the applied voltage, which can be due to the narrow Schottky barrier width that creates a significant tunneling current, thus decreasing the sensitivity.

On the other hand, responsivity ($\Re$) is a key factor that is

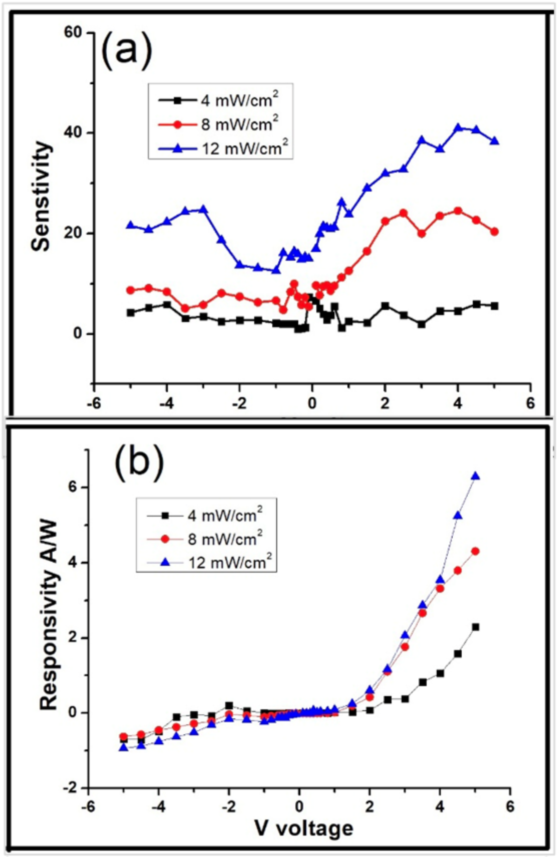

Fig. 7 (a) Sensitivity and Responsivity of Au/Sb_2O_3-nanosheet/Au device as a function of applied voltage under different intensity of light

typically detailed by the company that manufactures the photodetector, because it determines the quantum efficiency of the detector which in turn is considered as one of the

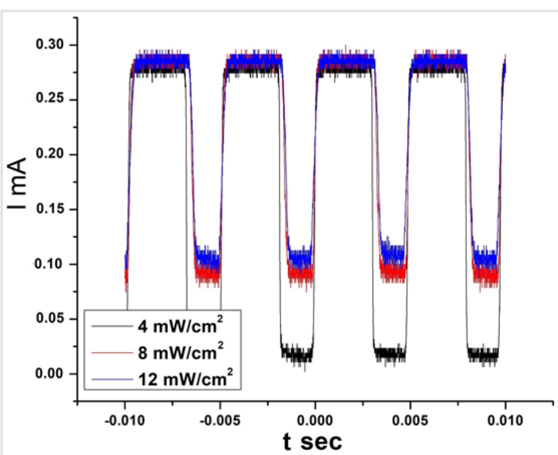

Fig. 8 Repeatability dynamic response (on/off) of the time-dependent photovoltage signal of the Sb_2O_3 nanoparticles sensor measured at different intensity of illuminated UV light.

photodetector figures of merit, through the equation:

$$\eta = R.hv/q \quad \ldots\ldots. (4)$$

where η, , v *and* q are efficiency, plank's constant, frequency of incident light, and electron charge.

Responsivity ($\Re$) is defined as the ratio of output current to optical power input. $\Re$ measures the efficiency of the detector in converting EM radiation to electrical current. It depends on temperature, wavelength, and bias voltage. This is the most important characteristic when considering the bias of the detector. $\Re$ can be expressed as;

$$\Re = \frac{I_{ph}}{P_{op}} \quad \ldots\ldots\ldots\ldots \quad (4)$$

where P_{op} is the absorbed power by (active material).

Fig. 7 (b) shows the responsivity of the MSM device at different UV intensities (4, 8, 12) mW/cm^2 with bias voltage in the range of (-5 to +5) V. The device exhibited a higher responsivity (in forwarding bias) and increased while increasing the bias voltage. This may be due to the steady increase of the photocurrent. Because beyond the potential barrier, the higher voltage reduces the barrier and enhances the flow of electrons, resulting in higher responsivity. These phenomena are affected also by types of substrates as well as electrodes. However, when a negative voltage was applied to Au, the Au/Sb_2O_3 reverse junction dominated the behavior of the Sb_2O_3 MSM detector. Since Au has a high work function, there will be no obvious net charge associated with trapped holes, and hence no reduction in the Schottky barrier height at the Au/ Sb_2O_3 interface, leading to the lower responsivity as shown in Fig. 7b. Measurements of the present work indicate that Au/Ultrathin Sb2O3/Au have a relatively low responsivity compared to other Schottky barrier UV detectors as shown in table (1). The device showed maximum value of responsivity of approximately 6 with a 5V bias. Table (I) shows the calculated sensitivity and responsivity for $Au/Sb_2O_3/Au$ photodetectors illuminate with different intensity of UV-395 nm and at different bias voltages, as well as results of other similar works.

3.4-Response time analysis

The key determining parameters of the performance of a photodetector or light sensor are response speed and repeatability [40]. And it considered as an important Figure of Merit of UV detectors. As illustrated in Fig. 1, part (b) of the system is used for current-time (I-t) measurements to calculate repeatability and response of $Au/Sb_2O_3/Au$ photo sensor. Across a number of cycles of switching the light source 'on' and 'off', the device (Figure 8) displayed excellent stability under different UV intensities (4, 8, 12) mW/cm^2 measured at dc bias voltage of +5 V.

The response time is the requisite time for the photocurrent to rise from 10% to 90% of I peak (peak photocurrent). The recovery time is similarly defined. The output current-time signals observed in Fig. 8 were utilized for the determination of response and recovery times under ambient environment. The calculated responsivity and sensitivity values are presented in table (I).

Table (I) shows the calculated sensitivity and responsivity of Au/Sb_2O_3/Au device compare with other works with their bias voltages measured at different power intensity of illumined light.

Configuration	Intensity of UV (mW/cm^2)	Wave length (nm)	Bias voltage (V)	Sensitivity	Responsivity (W/A)	Rise time (msec)	Fall time (msec)	Reference
Au/Sb_2O_3-nanosheet/Au	4	395	+1	2.56	0.016			This work
			+3	1.95	0.384			
			+5	5.64	2.298	0.32	0.24	
	8		+1	12.56	0.017			
			+3	19.99	1.76			
			+5	20.38	4.311	0.27	0.17	
	12		+1	23.8	0.091			
			+3	38.54	2.066			
			+5	38.37	6.294	0.11	0.067	
Au/ Sb_2O_3 (nanobelt)/Au	2.5	400	20	-	-	0.3	0.3	15
Sb_2O_3/Ag/Sb_2O_3	--	376	external quantum efficiency (EQE) of 4.1% with the maximum output power density of 5.18 mW cm^{-2}			---	---	14
Ag/n-ZnO NRs/Ag	150	360	-4	-	0.38	11	14	34
Ni/GaN/Au	-	370	5	-	1.13	-	-	35
Ti/$K_2Nb_8O_{21}$/Au	0.12	320	5	-	2.53	0.3	0.3	36
(Cr-Au) /Nb_2O_5/(Cr-Au) /	0.91	320	1	-	15.2	4	9	37
Au/ZnO film/Pt	15	325	3	-	24	1	45	38
Au/ZnONWs/Au	0.5	370	10	-	40	0.67	1.02	39

It is discernible that both rise and fall times decrease as the light intensity increases. Rise and fall times of 0.113 and 0.672 msec, respectively, were recorded at $12mW/cm^2$. The rapid and reversible switching between the illumination being 'on' or 'off' is the figure of merit on which we depend on to consider the sensor as a high-performance UV-Photodetector, and confirms the potential application of these sensors in the manufacture of advanced photosensitive switches. Fig (8) also shows the minimum and maximum values of the photocurrent versus time at intensities of (4, 8, 12) mW/Cm2, wavelength of 395 nm, and 5-volt bias operation. Neglecting the current distortion (noise), the minimum values of photocurrent agree with the results of fig. (6). This means that the chopper did not totally block the light from the source, when it is in a closed state. As for higher values of the photocurrent, which seem to be equal when the chopper is in the open state. Two phenomena can be observed, first, an increase in the value of the photocurrent, which usually results from an increase in light power.his may happen as a result of the constructive interference of direct incident light and the light incident through the slit hole of the chopper. Second, the photocurrent of the detector has reached a saturated state, which means that the incident power exceeds a certain limit that the photo-generated charge density approaches a certain device-specific value cause to reduce the photodiode's internal potential, so the photodiode response becomes saturated. The above two phenomena need a deeper study and will be the subject of our next research.

The measured sensor parameters of the (Au/Sb_2O_3/Au) based on fabricated UV MSM photodetector compared with other reported data for different MSM structures are summarized in Table (I). It can be deduced that the device produced in this study demonstrates a relatively good sensitivity and responsivity with fast response and recovery time. These significant results could be attributed to two factors. Firstly, the high value of surface to volume ratio of ultrathin Sb_2O_3 nanosheet helps to increase the absorption of light inside the film, thus improving the generation of photocurrent. Secondly, the interdigitated Schottky contact of Au with Sb_2O_3 provides a significant barrier height that results in small leakage current and high breakdown voltage, which, in turn, could improve the responsivity and photocurrent to dark current contrast ratio. These phenomena explain the high-performance of MSM UV photodiodes. These results demonstrate that the fabricated Au/Sb_2O_3/Au device is very sensitive to UV-light.

Conclusion

In Conclusion, a fast response and recovery times of 113.6 ms and 67.2 ms, considerable sensitivity and responsitivity, and high on/off ratio toward light at intensities of $12mW/cm^2$, wave length region of 395nm and 5 Volt bias operation was realized by using a Schottky barrier Au/Sb_2O_3 Ultrathin Nanosheet/Au MSM UV detector which fabricated successfully by solvothermal technology using ethanol as a solvent. The rapid and reversible switching between the illumination being 'on' or 'off' confirms the potential application of these sensors in the manufacture of advanced photosensitive switches. Therefore, this study supports a passage for design of high sense Au/Sb2O3/Au UV detector. It was also concluded that the responsivity varied with the polarity of the applied voltage; a higher responsivity was obtained when a positive voltage was applied at the Au/Sb2O3 contact.

Conflict of Interest

The author declare that they have no conflict of interest

Reference

N. N. Jandow, H. A. Hassan, F. K. Yam, and K. Ibrahim, *ZnO Metal-Semiconductor-Metal UV Photodetectors on PPC Plastic with Various Metal Contacts*, Photodetectors 1 (2012).

A. F. Abdulrahman, S. M. Ahmed, A. A. Barzinjy, S. M. Hamad, N. M. Ahmed, and M. A. Almessiere, *Fabrication and Characterization of High-Quality UV Photodetectors Based ZnO Nanorods Using Traditional and Modified Chemical Bath Deposition Methods*, Nanomaterials **11**, 677 (2021).

J. C. Carrano, P. A. Grudowski, C. J. Eiting, R. D. Dupuis, and J. C. Campbell, *Very Low Dark Current Metal--Semiconductor--Metal Ultraviolet Photodetectors*

Fabricated on Single-Crystal GaN Epitaxial Layers, Appl. Phys. Lett. **70**, 1992 (1997).

L. Qi, K. R. C. Mok, M. Aminian, E. Charbon, and L. K. Nanver, *UV-Sensitive Low Dark-Count PureB Single-Photon Avalanche Diode*, IEEE Trans. Electron Devices **61**, 3768 (2014).

B. Pandit and J. Cho, *AlGaN Ultraviolet Metal--Semiconductor--Metal Photodetectors with Reduced Graphene Oxide Contacts*, Appl. Sci. **8**, 2098 (2018).

H. Chang, D. H. Lee, H. S. Kim, J. Park, and B. Y. Lee, *Facile Fabrication of Self-Assembled ZnO Nanowire Network Channels and Its Gate-Controlled UV Detection*, Nanoscale Res. Lett. **13**, 1 (2018).

X. Sun, F. Azad, S. Wang, L. Zhao, and S. Su, *Low-Cost Flexible ZnO Microwires Array Ultraviolet Photodetector Embedded in PAVL Substrate*, Nanoscale Res. Lett. **13**, 1 (2018).

X. Liu, L. Gu, Q. Zhang, J. Wu, Y. Long, and Z. Fan, *All-Printable Band-Edge Modulated ZnO Nanowire Photodetectors with Ultra-High Detectivity*, Nat. Commun. **5**, 1 (2014).

Y. Xie, L. Wei, G. Wei, Q. Li, D. Wang, Y. Chen, S. Yan, G. Liu, L. Mei, and J. Jiao, *A Self-Powered UV Photodetector Based on TiO 2 Nanorod Arrays*, Nanoscale Res. Lett. **8**, 1 (2013).

X. Li, C. Gao, H. Duan, B. Lu, X. Pan, and E. Xie, *Nanocrystalline TiO2 Film Based Photoelectrochemical Cell as Self-Powered UV-Photodetector*, Nano Energy **1**, 640 (2012).

W. Tian, C. Zhang, T. Zhai, S.-L. Li, X. Wang, M. Liao, K. Tsukagoshi, D. Golberg, and Y. Bando, *Flexible SnO 2 Hollow Nanosphere Film Based High-Performance Ultraviolet Photodetector*, Chem. Commun. **49**, 3739 (2013).

Y. Zhang, T. Ji, W. Zhang, G. Guan, Q. Ren, K. Xu, X. Huang, R. Zou, and J. Hu, *A Self-Powered Broadband Photodetector Based on an n-Si (111)/p-NiO Heterojunction with High Photosensitivity and Enhanced External Quantum Efficiency*, J. Mater. Chem. C **5**, 12520 (2017).

R. Zou, Z. Zhang, Q. Liu, J. Hu, L. Sang, M. Liao, and W. Zhang, *High Detectivity Solar-Blind High-Temperature Deep-Ultraviolet Photodetector Based on Multi-Layered (L00) Facet-Oriented $β$-Ga2O3 Nanobelts*, Small **10**, 1848 (2014).

C. Song, N. Zhang, J. Lin, X. Guo, and X. Liu, *Sb 2 O 3/Ag/Sb 2 O 3 Multilayer Transparent Conducting Films for Ultraviolet Organic Light-Emitting Diode*, Sci. Rep. **7**, 1 (2017).

L. Li, Y. X. Zhang, X. S. Fang, T. Y. Zhai, M. Y. Liao, H. Q. Wang, G. H. Li, Y. Koide, Y. Bando, and D. Golberg, *Sb2O3 Nanobelt Networks for Excellent Visible-Light-Range Photodetectors*, Nanotechnology **22**, 165704 (2011).

Q. Wang, X. Yang, J. Hou, M. Huang, and Y. Zhao, *Hydrothermal Synthesis of Sb2O3 Nanorod-Bundles via Self-Assembly Assisted Oriented Attachment*, Appl. Surf. Sci. **257**, 5857 (2011).

Y. Zhang, G. Li, and L. Zhang, *Growth of Sb2O3 Nanotubes via a Simple Surfactant-Assisted Solvothermal Process*, Chem. Lett. **33**, 334 (2004).

K. V Divya and K. E. Abraham, *Ag Nanoparticle Decorated Sb2O3 Thin Film: Synthesis, Characterizations and Application*, Nano Express **1**, 20005 (2020).

N. M. A. Hadia, S. Garc\'\ia-Granda, and J. R. Garc\'\ia, *Structural and Optical Properties of Hydrothermally-Synthesized Single-Crystalline Sb 2 O 3 Nanowires*, J. Korean Phys. Soc. **63**, 2143 (2013).

Z. Deng, F. Tang, D. Chen, X. Meng, L. Cao, and B. Zou, *A Simple Solution Route to Single-Crystalline Sb2O3 Nanowires with Rectangular Cross Sections*, J. Phys. Chem. B **110**, 18225 (2006).

L. Song, S. Zhang, and Q. Wei, *Antimony Trioxide Microstructures: 3D Grass-like Architectures and Optical Properties*, Chem. Eng. J. **179**, 404 (2012).

S. Ge, Q. Wang, Q. Shao, Y. Zhao, X. Yang, and X. Wang, *Hydrothermal Synthesis of Morphology-Controllable Sb2O3 Microstructures: Hollow Spindle-like and Cobblestone-like Microstructures*, Appl. Surf. Sci. **257**, 3657 (2011).

J. Wu, P. Qiao, H. Li, Y. Xu, W. Yang, F. Yang, K. Lin, K. Pan, and W. Zhou, *Engineering Surface Defects on Two-Dimensional Ultrathin Mesoporous Anatase TiO 2 Nanosheets for Efficient Charge Separation and Exceptional Solar-Driven Photocatalytic Hydrogen Evolution*, J. Mater. Chem. C **8**, 3476 (2020).

R. Köferstein, L. Jäger, and S. G. Ebbinghaus, *Magnetic and Optical Investigations on LaFeO3 Powders with Different Particle Sizes and Corresponding Ceramics*, Solid State Ionics **249**, 1 (2013).

T. P. McLean, *The Absorption Edge Spectrum of Semiconductors*, Prog. Semicond. **5**, i960 (1960).

M. M. Furchi, D. K. Polyushkin, A. Pospischil, and T. Mueller, *Mechanisms of Photoconductivity in Atomically Thin MoS2*, Nano Lett. **14**, 6165 (2014).

F. So, *World Scientific Handbook Of Organic Optoelectronic Devices (Volumes 1 \& 2)*, Vol. 12 (World Scientific, 2018).

R. Shabannia, H. A. Hassan, H. Mahmodi, N. Naderi, and H. R. Abd, *ZnO Nanorod Ultraviolet Photodetector on*

Porous Silicon Substrate, Semicond. Sci. Technol. **28**, 115007 (2013).

L. Li, P. Wu, X. Fang, T. Zhai, L. Dai, M. Liao, Y. Koide, H. Wang, Y. Bando, and D. Golberg, *Single-Crystalline CdS Nanobelts for Excellent Field-Emitters and Ultrahigh Quantum-Efficiency Photodetectors*, Adv. Mater. **22**, 3161 (2010).

J. A. Dirksen, K. Duval, and T. A. Ring, *NiO Thin-Film Formaldehyde Gas Sensor*, Sensors Actuators B Chem. **80**, 106 (2001).

Y. K. Su, S. J. Chang, C. H. Chen, J. F. Chen, G. C. Chi, J. K. Sheu, W. C. Lai, and J. M. Tsai, *GaN Metal-Semiconductor-Metal Ultraviolet Sensors with Various Contact Electrodes*, IEEE Sens. J. **2**, 366 (2002).

S.-J. Young, L.-W. Ji, S.-J. Chang, and Y.-K. Su, *ZnO Metal--Semiconductor--Metal Ultraviolet Sensors with Various Contact Electrodes*, J. Cryst. Growth **293**, 43 (2006).

S. Zhang, D. G. Zhao, D. S. Jiang, W. B. Liu, L. H. Duan, Y. T. Wang, J. J. Zhu, Z. S. Liu, S. M. Zhang, and H. Yang, *Investigation of Responsivity Decreasing with Rising Bias Voltage in a GaN Schottky Barrier Photodetector*, Semicond. Sci. Technol. **23**, 105015 (2008).

N. H. Al-Hardan, A. Jalar, M. A. A. Hamid, L. K. Keng, N. M. Ahmed, and R. Shamsudin, *A Wide-Band UV Photodiode Based on n-ZnO/p-Si Heterojunctions*, Sensors Actuators A Phys. **207**, 61 (2014).

D. Li, X. Sun, H. Song, Z. Li, H. Jiang, Y. Chen, G. Miao, and B. Shen, *Effect of Asymmetric Schottky Barrier on GaN-Based Metal-Semiconductor-Metal Ultraviolet Detector*, Appl. Phys. Lett. **99**, 261102 (2011).

H. Liu, Z. Zhang, L. Hu, N. Gao, L. Sang, M. Liao, R. Ma, F. Xu, and X. Fang, *New UV-A Photodetector Based on Individual Potassium Niobate Nanowires with High Performance*, Adv. Opt. Mater. **2**, 771 (2014).

X. Fang, L. Hu, K. Huo, B. Gao, L. Zhao, M. Liao, P. K. Chu, Y. Bando, and D. Golberg, *New Ultraviolet Photodetector Based on Individual Nb2O5 Nanobelts*, Adv. Funct. Mater. **21**, 3907 (2011).

C. Y. Liu, B. P. Zhang, Z. W. Lu, N. T. Binh, K. Wakatsuki, Y. Segawa, and R. Mu, *Fabrication and Characterization of ZnO Film Based UV Photodetector*, J. Mater. Sci. Mater. Electron. **20**, 197 (2009).

L. Guo, H. Zhang, D. Zhao, B. Li, Z. Zhang, M. Jiang, and D. Shen, *High Responsivity ZnO Nanowires Based UV Detector Fabricated by the Dielectrophoresis Method*, Sensors Actuators B Chem. **166**, 12 (2012).

Y. Zou, Y. Zhang, Y. Hu, and H. Gu, *Ultraviolet Detectors Based on Wide Bandgap Semiconductor Nanowire: A Review*, Sensors **18**, 2072 (2018).

W. Jin, Y. Ye, L. Gan, B. Yu, P. Wu, Y. Dai, H. Meng, X. Guo, and L. Dai, *Self-Powered High Performance Photodetectors Based on CdSe Nanobelt/Graphene Schottky Junctions*, J. Mater. Chem. **22**, 2863 (2012).